Journal of Marine Research, 58, 269–295, 2000

Mechanism of eddy separation from coastal currents

by Melvin E. Stern[1] and Eric P. Chassignet[2]

ABSTRACT

A series of multi-layer numerical experiments show that classical finite amplitude instabilities in boundary currents are not sufficient to account for the pinched-off eddies observed in the ocean and in laboratory experiments. These instabilities (barotropic or baroclinic) are shown to lead to an *entrainment* of offshore fluid into the boundary currents. Eddy separation, on the other hand, requires an additional process, such as a larger scale of motion containing a downstream velocity convergence of finite amplitude; this might be produced by long period fluctuations in the discharge from an upstream source region which controls the boundary current, or by topographic features. In our spatially idealized model, we numerically computed the temporal evolution of an assumed initial state consisting of a fast moving upstream region separated by a potential vorticity front from a slow moving downstream region. We verify long-wave theories which show that this initial state indeed leads to frontal steepening and to a blocking wave. This eventually produces large transverse velocities followed by complete *detrainment* of eddies without any *entrainment* into the residual boundary current.

1. Introduction

The separation of ocean eddies from continental boundary currents can result from many different, and not yet fully explained, factors. One example is the Meddies, which intermittently detach from part of the Mediterranean outflow while the remainder of the jet continues flowing along the Iberian continental slope (Bower *et al.,* 1997; Stern, 1999; Jungclaus, 1999). Another example is the "squirts and filaments," which separate from the California coastal current [see Haidvogel *et al.* (1991) and the companion articles in the same journal volume]. Although barotropic and baroclinic instabilities are important in the latter, Haidvogel *et al.* (1991) have shown that it is not sufficient to account for the filaments, since they disappear when the *irregular* coastal topography in the numerical model is removed. In that case, only the barotropic and baroclinic instability of the undisturbed jet appear, and these do not form pinched-off eddies. A similar result was obtained by Jiang and Garwood (1998) in a numerical calculation in which a density current flows down a uniformly sloping bottom in a uniformly stratified environment. In that calculation, the large-scale eddies generated by instability cause *entrainment* and

1. Department of Oceanography, Florida State University, Tallahassee, Florida, 32306-4320, U.S.A. ***email: stern@ocean.fsu.edu***

2. RSMAS/MPO, University of Miami, 4600 Rickenbacker Causeway, Miami, Florida, 33149, U.S.A.

mixing with the ambient fluid until the jet reaches its own density level, whereupon it flows parallel to the slope isobaths as a nearly laminar jet. The initial baroclinic eddies serve only to mix ambient fluid and to produce a robust downstream jet with no detached eddies. Note that even in the well-known case of a highly unstable free barotropic jet (no walls), the periodic array of dipolar vortices generated on both sides of the jet axis do not continually propagate away from the axis, but curve back and become an integral part of the new mean jet flow (Flierl *et al.,* 1987). Likewise for the classical three-dimensional flow of a uniform density jet emerging from a nozzle; the experimentally observed eddies (Wygnanski *et al.,* 1992) do not permanently separate into the irrotational surrounding fluid, but entrain it, so that the turbulent eddies constitute an integral part of the diffusing downstream jet.

Separation of fluid from the boundary jet (or *detrainment*) has been observed in laboratory experiments without any topographic features. Baey *et al.* (1995) introduced a flow along the sidewall of a rotating tank between two density layers initially at rest; the injected fluid is of intermediate density and represents an idealization of the Mediterranean outflow. The most striking feature in some (but not all) of these experiments is the formation of separated lenses and dipoles associated with a pronounced flux in the direction perpendicular to the wall current.

In another series of laboratory experiments (Stern, 1980; Stern *et al.,* 1997), a low density jet (dyed) is pumped through a source whose open top lies slightly below the free surface of a relatively deep and more saline fluid. As in the experiments of Baey *et al.* (1995), the Coriolis force deflects the discharge toward the wall, along which it flows as a narrow jet (with a low Froude number). For various physical reasons, the maximum velocity decreases downstream, and very small values occur near the distant leading edge of the dyed intrusion. Immediately upstream from this edge, there appears a periodic group of typical finite amplitude instability waves (Griffiths and Linden, 1981), but farther upstream near the source there are much larger disturbances containing fluid parcels that have been ejected from the wall and penetrated to a distance that is an order of magnitude larger than the undisturbed width of the laminar wall current. It appears that at an earlier time these large eddies (possibly initiated by baroclinic instability) block the oncoming thin laminar jet, thereby diverting part of the source flow into the interior of the tank, and decreasing the downstream transport of fresh water along the wall. Such a process (or the lack of it) is obviously of general interest for ocean mixing. A similar process takes place in the numerical experiment of Jungclaus (1999) in which the quasi-laminar slope current from the source was blocked by the nose of the density intrusion. The strong convergence of downstream velocities led to the formation of a baroclinic dipole which detaches from the slope. The cyclonic partner eventually dissipated, leaving behind only an anticyclone (meddy-like).

In this paper, we try to isolate one mechanism for the aforementioned detrainment (i.e., complete separation of fluid from the boundary jet), and contrast it with the opposite effect, viz. entrainment. The outline of the paper is as follows. The finite amplitude instability of a wall jet in a 1½ layer density model is first considered in Section 2a, and then, in Section

2b, a 3-layer jet with a surfacing density front is considered. In both cases, small amplitude *periodic* downstream disturbances will be shown numerically to lead to *entrainment* of ambient fluid into the wall jet, but no eddy separates from the boundary current. For the purpose of isolating our proposed separation mechanism, a quite different set of initial conditions is assumed in Sections 3 and 4, viz. one in which the downstream current varies by a large amount over a small downstream distance. We study the circumstances when the initially small transverse velocities can be amplified, thereby diverting the boundary current into the interior. Using a longwave approximation, analytical theories of blocking waves in rotating boundary currents are reviewed in Section 3. Section 4 extends the latter calculation by adopting the 1½ layer and 3-layer numerical models introduced in Section 2; some of the conditions favorable to eddy separation are then discussed and summarized in Section 5.

2. Entrainment by instability in density stratified boundary jets

In this section, it will be shown that finite amplitude instabilities are generally not sufficient to account for the pinched-off eddies that are observed to form in the ocean and in the laboratory experiments cited above. Small amplitude periodic downstream perturbations ($\sim$ fastest growing) of the unstable boundary current only lead to entrainment of ambient (offshore) fluid into the wall jet, beyond which no separated eddy appears.

a. Entrainment in an unstable 1½ layer wall jet

The instability of a rotating and density stratified fluid is due to a combination of the kinetic and potential energy releasing mechanisms. In this section, we first consider a 1½ layer jet in which the lateral shear (i.e., the first mechanism) is of primary importance. This model, in which potential vorticity is conserved, is, in the quasi-geostrophic limit, similar in many respects to the pure *barotropic* wall jet in which relative vorticity is conserved. In the latter case, Stern *et al.* (1997) computed the fastest growing periodic disturbance for a piecewise uniform *vorticity* flow whose basic velocity profile consisted of an isosceles triangle. A numerical calculation was then performed to show that, although the dipolar vortices which evolved from the amplifying normal mode do start to propagate away from the wall, the dipoles eventually curve back and merge inside a widened mean flow wall, as is the case with a free jet (Flierl *et al.,* 1987). In this barotropic process, the eddies entrain irrotational fluid from the far field, rather than separating from the new mean boundary flow.

In order to show that a similar effect occurs for a 1½ layer quasi-geostrophic wall jet with piecewise uniform *potential* vorticity, we consider that the undisturbed velocity (Eqs. 2–4, below) has a maximum at $y = L_1$, and vanishes at both $y = 0$ and at $y = L_1 + L_2$. All length units here are made nondimensional using the radius of deformation as the length scale, and the maximum undisturbed velocity at $y = L_1$ provides the velocity scale; the basic velocity profile is then completely given in quasi-geostrophic theory in terms of

hyperbolic functions. The perturbation eigenfunctions, therefore, have piecewise vanishing perturbation potential, and these eigenfunctions are connected in the usual way across the discontinuities ($y = L_1$, $y = L_1 + L_2$). An extensive calculation yields the following eigenvalue equation

$$0 = c^2[\Gamma + \Gamma \coth(\Gamma L_1)] - c\left[\Gamma + \frac{e^{-\Gamma L_2}\cosh(\Gamma L_2)}{\sinh(L_2)} + \frac{e^{-\Gamma L_2}\sinh(L_2\Gamma)\coth(\Gamma L_1)}{\sinh(L_2)} - \Gamma\left(\frac{\coth(L_2) + \coth(L_1)}{\Gamma} - \coth(L_1)\right)\right] + \frac{e^{-\Gamma L_2}\cosh(L_2\Gamma)}{\sinh(L_2)} - \left(\frac{\coth(L_2) + \coth(L_1)}{\Gamma} - \coth(\Gamma L_1)\right)\frac{e^{-\Gamma L_2}\sinh(L_2\Gamma)}{\sinh(L_2)} \quad (1)$$

for the complex phase speed c of wavenumber k, where $\Gamma = (1 + k^2)^{1/2}$. For $L_2 = 1.0$ and $L_1 = 0.7$, the wavenumber of fastest growth is $k = 1.26$, and the phase separation between the crests of the two interfaces is 1.045 rads.

The finite amplitude behavior is investigated by configuring the Miami Isopycnic Coordinate Ocean Model (MICOM, cf. Bleck and Boudra, 1986; Bleck and Chassignet, 1994) as a 1½ layer (not quasi-geostrophic) model in a numerical domain of non-dimensional width and length $\lambda = 10$ (Fig. 1); the first harmonic then has a $k = 2\pi/5$ close to the fastest growing $k = 1.26$. The grid spacing was 0.05 and a small Newtonian viscosity of 5×10^{-4} was used in the momentum equations (with free slip boundary conditions). The undisturbed downstream velocity profile for piecewise uniform potential vorticity (hereafter referred to as PV) is

$$u = \cosh(y - L_1) + \sinh(y - L_1)\coth(L_1), \qquad y \le L_1 = 0.7 \quad (2)$$

$$u = \cosh(y - L_1) - \sinh(y - L_1)\coth(L_2), \qquad L_1 \le y \le L_1 + L_2 = 1.7 \quad (3)$$

$$u = 0, \qquad L_1 + L_2 \le y \le \lambda \quad (4)$$

and the associated *initial* thickness anomaly, h, was computed geostrophically. The remaining parameters (Coriolis parameter, f; reduced gravity, g'; and undisturbed layer thickness, H_o) were chosen so that the finite Rossby number (based on the radius of deformation R_d) was 0.1. A small amplitude cross-stream velocity $v = 0.1\cos(2\pi x/\lambda)$, added at $t = 0$, provided the perturbation.

Figure 1a shows the departure at $t = 20$ of PV from f/H_o (the *absolute* value of PV has no dynamical significance). Although the initial disturbance did not have the y-dependence of the eigenfunction (Eq. 1), and although PV diffuses from piecewise uniformity because of viscosity, the downstream phase difference between wave crests at $t = 15$ agreed with the value predicted by the foregoing quasi-geostrophic instability theory. At $t = 50$ (Fig. 1b), the sinusoidal perturbation rolls up into dipolar potential vortices that start to travel away from the wall, but do not continue doing so. This can be clearly seen in Fig. 1c ($t = 100$), in which the exterior fluid with PV = 0 is irreversibly entrained into the new mean flow, and

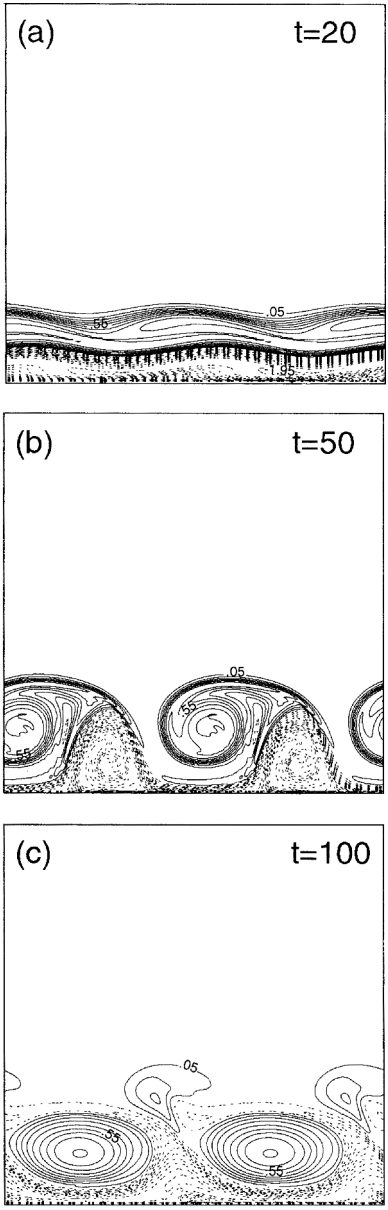

Figure 1. Potential vorticity departure from f/H_o for the 1½ layer numerical simulation of Section 2a: (a–c) $t = 20, t = 50, t = 100$.

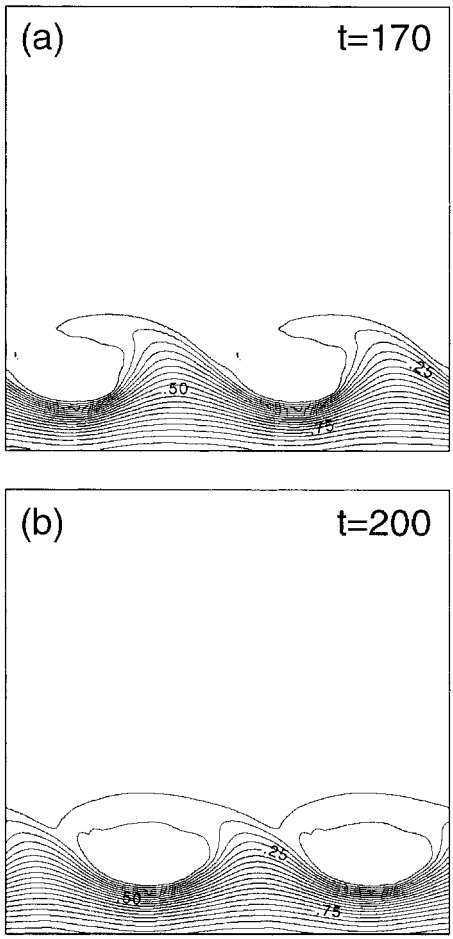

Figure 2. Layer thickness h_2 contours for the 3-layer numerical simulation of Section 2b (contour interval of 0.05): (a–b) $t = 170, t = 200$ for the harmonic run; (c–f) $t = 145, t = 200, t = 250, t = 400$ for the combined harmonic and subharmonic run. Bottom layer vorticity for the 3-layer numerical simulation of Section 2b: (g) $t = 200$ for the harmonic and subharmonic run.

none of the (stippled) wall current leaves the boundary. Also noteworthy (but not shown) is the occurrence of a counter-gradient momentum flux after $t = 40$, at which time the outward (eddy) diffusion of the maximum mean velocity reverses.

b. Entrainment in an unstable baroclinic frontal jet

Instabilities involving release of potential energy can be modeled in a baroclinic frontal wall jet consisting of three density layers, each separated by the same density difference $\Delta\rho$, and such that the two interfaces surface at $y = L_1 = 1$ and $y = L_1 + L_2 = 2$, respectively. The length scale used in the nondimensionalization is the radius of deforma-

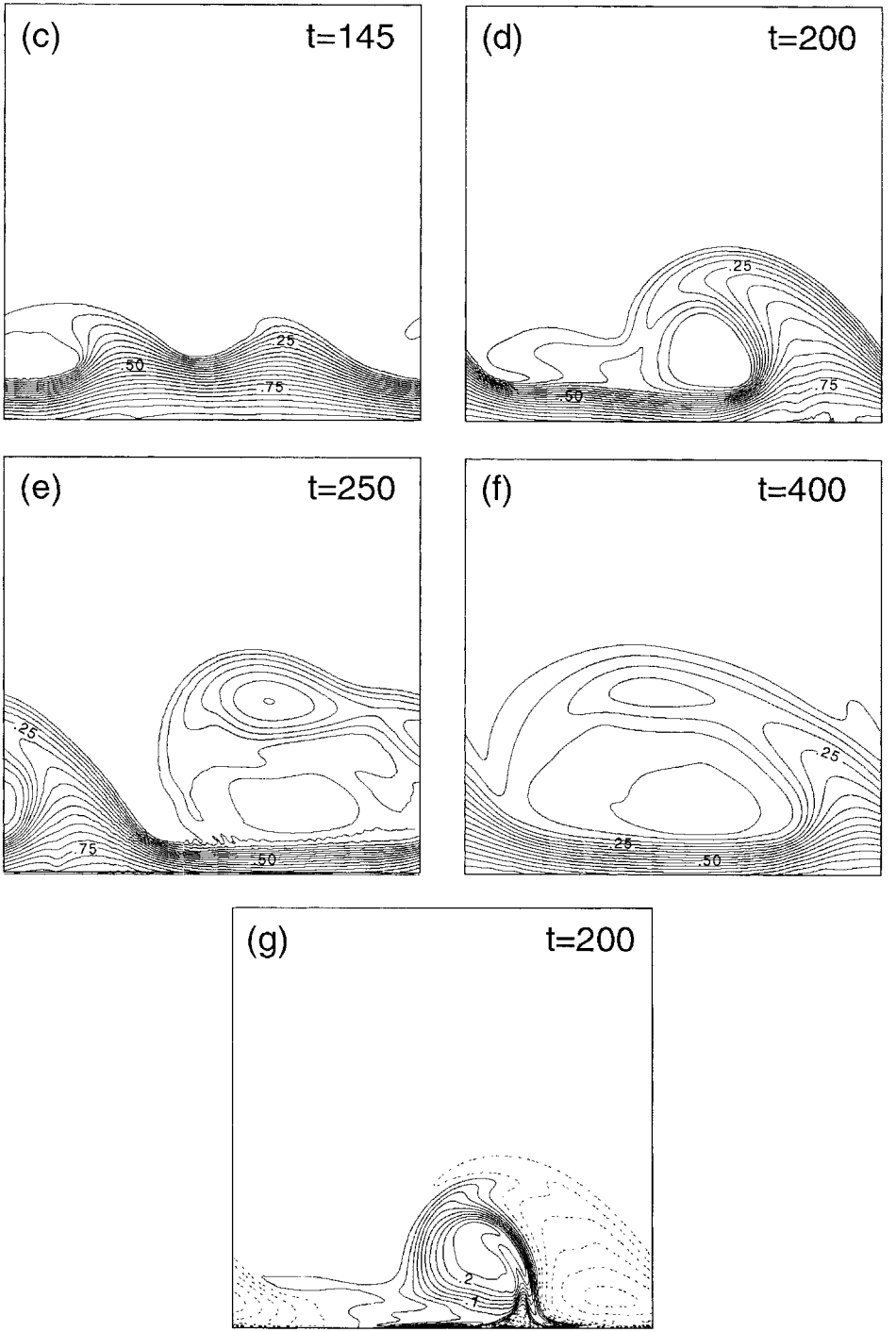

Figure 2. (Continued)

tion $R_d = (2g\Delta\rho/\rho H_o)^{1/2}/f$ based on the depth H_o at the wall of the lower interface of the intermediate density layer. The velocity scale is $U = 2gH_o(\Delta\rho/\rho)/fR_d$, and the bottom depth is $H = 5H_o$. The bottom layer is initially at rest, and the assumed initial non-dimensional thickness of the upper and lower interfaces are respectively given by

$$h_1 = \tfrac{1}{3}\,(1 + \cos(\pi y/L_1)), \qquad y \le L_1 \tag{5}$$

$$h_2 = \tfrac{1}{2}\,(1 + \cos(\pi y/(L_1 + L_2))), \qquad y \le L_1 + L_2. \tag{6}$$

The initial undisturbed geostrophic velocities are $u_2 = -\tfrac{1}{2}\partial h_2/\partial y$ and $u_1 = -\tfrac{1}{2}\partial h_1/\partial y - \tfrac{1}{2}\partial h_2/\partial y$. The computational domain for this run (Fig. 2) is identical to the previous one ($\lambda = 10$, $\Delta x = 0.05$), and the viscosity (5×10^{-4}) is the same in all three layers. Although we have no linear calculations for the fastest growing wave in this frontal model, a small amplitude initial perturbation with a wavelength $\lambda_W = 5$ was sufficient for our purpose. At $t = 170$ (Fig. 3a), the $h_2 = 0$ contour displays the typical "backward breaking wave" signature of a surfacing front (Griffiths and Linden, 1981). At $t = 200$ (Fig. 2b), entrainment of ambient (heavy) fluid inside the new mean flow is complete, and no light fluid is detrained outside this flow.

This run was repeated by adding at $t = 0$ a subharmonic of wavelength $\lambda_W = 10$, with an amplitude ⅓ of the previous disturbance. The results at $t = 145$ (Fig. 2c) and $t = 200$ (Fig. 2d) show the eventual dominance of the subharmonic, and clear entrainment. Although the dipolar vorticity in the bottom layer at this time (Fig. 2g) suggests that this might cause the entire eddy to propagate away from the wall, and eventually separate, this is clearly not the case as shown at $t = 250$ (Fig. 2e) and $t = 400$ (Fig. 2f). The net result of the instability is one of outward eddy *diffusion,* as relatively heavy fluid beyond the outcropping front is incorporated in the wall jet. It may be, however, that the inclusion of very long waves in a much larger computational domain will lead to localized detrainment events, similar to that found below.

3. Detrainment by blocking waves in boundary currents

The series of laboratory experiments performed by Stern (1980) and Stern *et al.* (1997) as well as the numerical experiments of Jungclaus (1999) strongly suggest that blocking and eddy separation can be induced by the intrinsic downstream variation in the jet emerging from a source; some aspect of the nonperiodic downstream variation of the wave disturbances seems to be necessary for eddy separation. In the ocean, other factors such as local topographic variations on the continental slope (Bower *et al.,* 1997) may induce eddy separation.

Blocking waves are familiar in the classical nonrotating problem of the uniform flow of a liquid with a free surface over an obstacle; an upstream propagating blocking wave is generated when the velocity above the obstacle becomes supercritical [Froude number greater than unity; see Pratt *et al.* (2000) for a review], so that part of the oncoming current does not flow over the obstacle, but forms an upstream propagating wave. Another

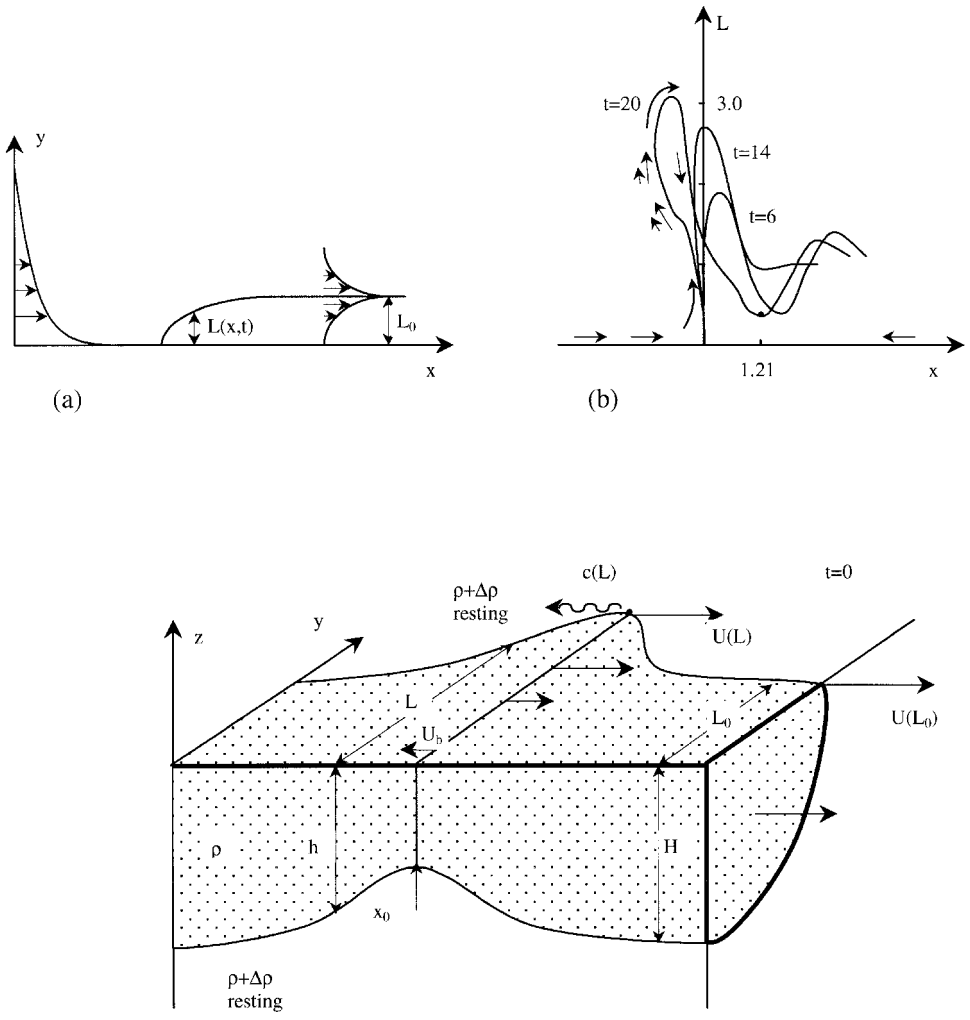

Figure 3. Schematic diagram of a piecewise uniform potential vorticity distribution ($t = 0$) leading to blocking. (a) $L(x, 0)$ is the initial distance from the wall ($y = 0$) of an interface bounding a relatively low PV domain, and the velocity distribution is such that a fast upstream wall current $[u(-\infty, 0)]$ approaches a slow downstream jet $[u(\infty, 0) = 0]$. (b) Evolution of $L(x, t)$ in a coordinate system moving with the "nose point" $L = 0$. The arrows indicate the intensity of particle motion along and around the interfacial contour. (c) Blocking wave in a surfacing density current flowing along a vertical wall. In the long wave approximation, the downstream velocity is geostrophic and the total transport at $x = x_o$ is less than at $x < x_o$. $U(L)$ is the velocity on the surfacing front, U_b is the velocity at the wall, and $c(L)$ is the local propagation velocity. As time increases the theory shows that the wave steepens ($\partial L/\partial x \to \infty$) at $x < x_o$, and the transverse velocity becomes as large as the downstream velocity ($U(L)$).

well-known example is the blocking wave which occasionally appears in the atmospheric troposphere, and which diverts the winds from their normal west to east path.

In the remainder of this paper, we investigate the blocking effect produced by a large amplitude local (essentially nonperiodic) disturbance in the jet. We will show that in some cases the convergent effect can be strong enough to cause fluid near the boundary wall to be rapidly ejected, and to form an eddy which completely pinches off from the remaining coastal current.

a. Theory of blocking waves in a 1½ layer quasi-geostrophic model

In the context of a 1½ layer quasi-geostrophic jet, a simple case of blocking (Stern, 1986) occurs when a "fast" flow region (emerging from an upstream source) converges on a downstream region with smaller near-wall velocities. The simplest idealization (Fig. 3a) of such an initial state is a jet represented by a current with uniform geostrophic potential vorticity (PV) inside an interface $L(x, t)$, and larger uniform PV ($= f/H$) outside, where H is the mean layer thickness. Far downstream (Fig. 3a), we specify a full jet profile with maximum nondimensional velocity $u(+\infty, L_o, t) = 1$ and with $u(x, 0, t) = 0$; the radius of deformation R_d provides the length scale. The velocity at $x = \infty$ is then equal to $e^{-(y-L_o)}$ for $y > L_o$, and $u(+\infty, y, t) = \sinh(y)/\sinh(L_o)$ for $y < L_o$. Far upstream, the maximum velocity of the uniform PV domain is near the wall, as specified by $u(-\infty, y, t) = h(-\infty, 0, t)e^{-y}$. Note that both the downstream and upstream laminar flows are geostrophically stable, so that the present model is well suited to isolate other finite amplitude effects (like blocking). Another advantage of this piecewise uniform PV model is that it allows, via contour dynamics, a relatively simple calculation (Stern, 1986) of the complete quasigeostrophic evolution of $L(x, t)$ in terms of a nonlinear integral equation (with Bessels K_o as the Greens function). If the initial L varies slowly downstream (i.e. longwave approximation), this integral equation reduces to the hyperbolic differential equation $\partial L/\partial t + c(L)\partial L/\partial x = 0$, where the propagation speed is

$$c(L) = -[\coth(L_o) - 1]e^{-L} + \coth(L_o)e^{-2L}$$

$$\frac{\partial c}{\partial L} = [\coth(L_o) - 1]e^{-L} - 2\coth(L_o)e^{-2L}.$$

Thus an observer initially at x who moves with speed $c(L)$ always sees the same initial value of $L(x, t) = L(x, 0)$. At small L (near the "nose" point), $C \to 1$, and since $\partial C/\partial L \to -[\coth(L_o)] < 0$, the nose ($L = 0$) propagates downstream faster than the fluid at larger x. Consequently, the slope of the nose front (or $\partial L/\partial x$) steepens in time and the offshore velocity $v > 0$ increases greatly compared to its relatively small initial value. This long wave approximation fails at the time when $\partial L/\partial x \to \infty$, and in order to compute the subsequent evolution (Fig. 3b), it was necessary to solve numerically the aforementioned integral (contour dynamical) equation. For this calculation, the assumed interfacial condition was $L(x, 0) = 1 - e^{-x}$, and a coordinate system whose origin ($x = 0$) moves with the nose point ($L = 0$) was used. The results (Fig. 3b) show that before $t = 5$, the

steepening of $\partial L/\partial x$ is qualitatively similar to that obtained with the longwave approximation. Subsequently $L(x, t)$ becomes multivalued, as a plume of low PV fluid from inside the interface is forced offshore. The slowly narrowing "neck" of the plume suggests that a pinched off ("detrained") eddy will eventually form for $t > 20$, but this long time behavior was not considered in this contour dynamics calculation. The suggested pinchoff will be verified in Section 4a using a finite difference numerical calculation with a small viscosity and with a continuous distribution of PV similar to the one depicted in Figure 3a.

b. Theory of blocking waves in an outcropping density front

A strongly ageostrophic example of blocking waves in an *outcropping* coastal front was also investigated in a longwave theory (Stern, 1980) for a 1½ layer shallow water model. This consists of a light upper layer with thickness $h(x, y, t)$, with uniform potential vorticity, and a motionless underlying layer (see Fig. 3c). The front (where $h = 0$) is located at a distance $y = L(x, t)$ from the wall ($y = 0$). In the assumed undisturbed state the frontal displacement $L(x, 0)$ equals a constant (L_o), and the downstream velocity $u(x, y, t)$ vanishes at $y = 0$. We then assume an initial finite amplitude longwave perturbation ($\partial h/\partial x \ll \partial h/\partial y$) such that $L(x, 0) \geq L_o$, and $h(x, 0, 0) \leq H$, where H is the layer thickness at $y = 0, x = \pm\infty$; the minimum downstream transport occurs at the minimum of $h(x, 0, 0)$. Using the method of characteristics, analytical solutions were obtained for the simplest case of zero potential vorticity (relative vorticity $= -f$), so that $u(x, y, t)$ decreases linearly with y, from $U(x, t) \equiv u(x, L, t)$ to $U_b(x, t) \equiv u(x, 0, t)$. Note that the cross stream velocity $v(x, y, t)$ is not geostrophically balanced so that $\partial h(x, 0, t)/\partial x \neq 0$ at the wall ($v = 0$); the total downstream transport can also vary with x (in contrast to the quasi-geostrophic case of Section 3a).

The general initial value problem, in which $h(x, 0, 0)$ and $L(x, 0)$ are *independently* specified, can be solved by the method of characteristics using two Riemann invariant functions $R_{\pm}[L(x, t), h(x, 0, t)]$, each of which retains its initial value relative to an observer moving with the corresponding propagation speed $c_{\pm}[L(x, t), h(x, t)]$. The Riemann functions in our problem can most easily be obtained from a "similarity" solution (of the momentum and continuity equations) of the form $h(x, 0, t) = F[L(x, t)]$, where the unknown function F is obtained by solving a time independent ordinary differential equation. Two such functions $[F_-, F_+]$ emerge, along with their associated propagation speeds $c_{\pm}[L(x, t)]$. One function (F_-) is such that, if $L > L_o$, then $h(x, 0, t) < H$, $c_-(L) < 0$, and $U_b < 0$. The initial state sketched in Figure 3c corresponds to the time invariant function F_-. It follows that the large values of $L(x, t)$ will propagate upstream [where $c_-(L_o) = 0$]; the upstream part of $L(x, t)$ steepens ($\partial L/\partial x \to \infty$), and the cross stream velocity v becomes as large as the downstream velocity u, at which point the longwave theory fails. It suggests, however, a typical blocking scenario which should eventually lead to a detached eddy. In order to investigate this possibility, a finite difference calculation will be presented in Section 4b.

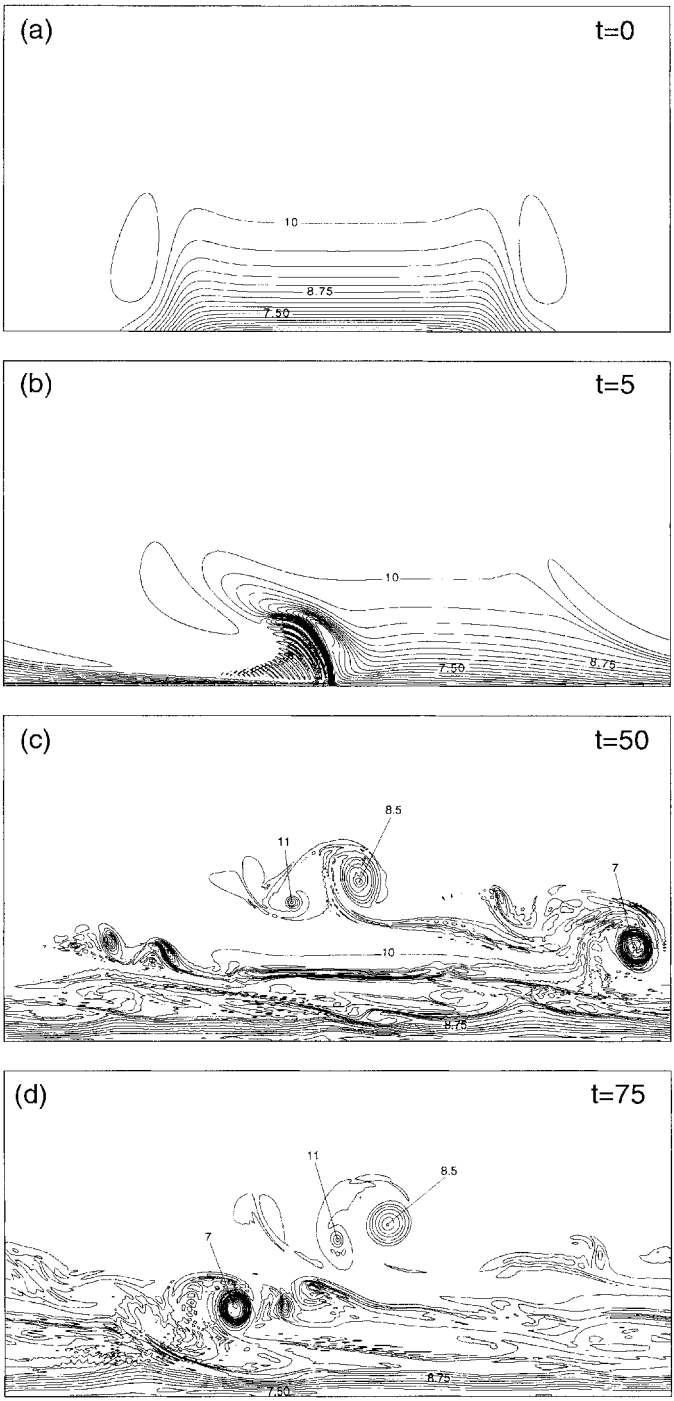

Figure 4. Potential vorticity contours for the first 1½ layer experiment of Section 4a (contour interval of 0.25): (a–d) $t = 0$, $t = 5$, $t = 50$, $t = 75$.

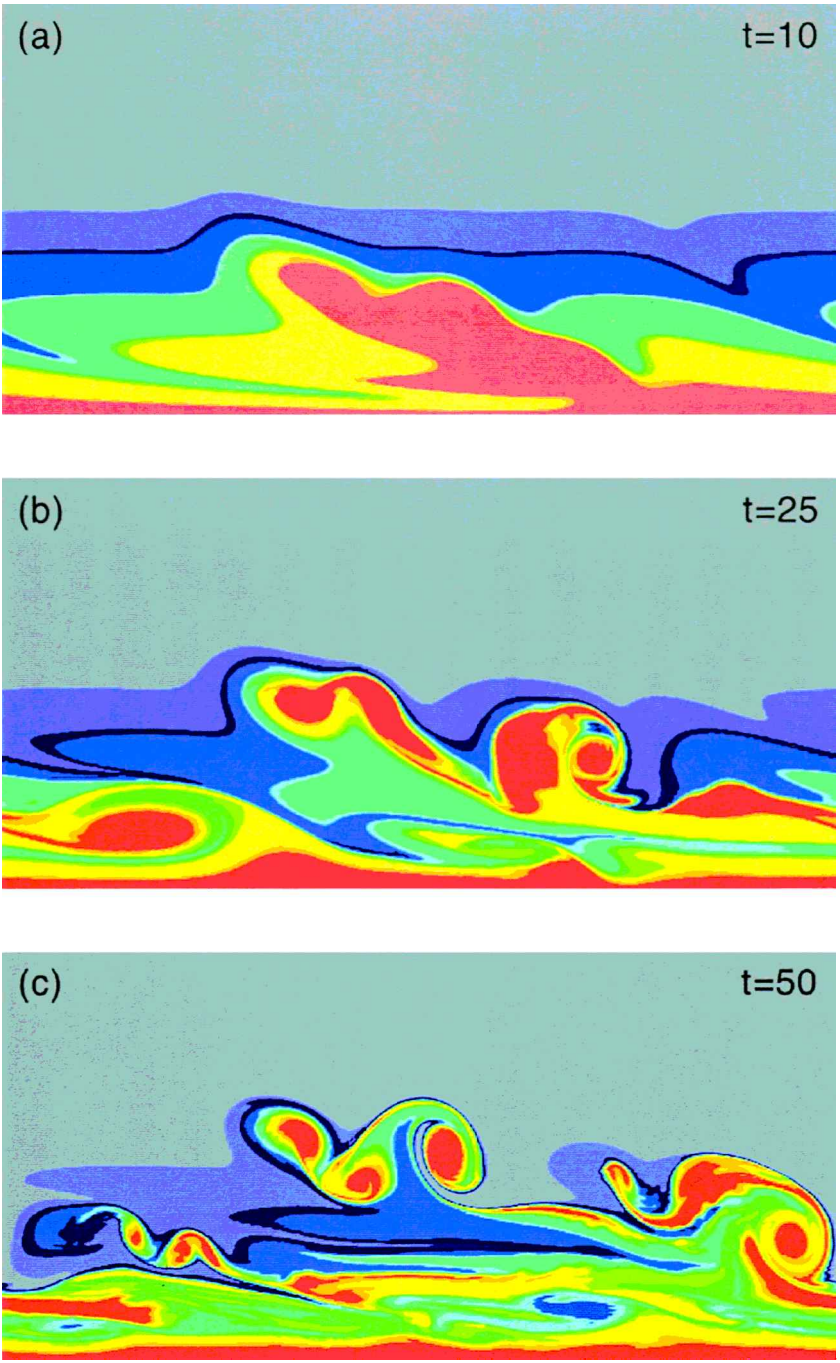

Figure 5. Time evolution of a passive tracer for the first 1½ layer experiment of Section 4a (injected at $t = 0$ over half the channel width such that there is a uniform band of color in x for every $\Delta y = 1$): (a–c) $t = 10$, $t = 25$, $t = 50$.

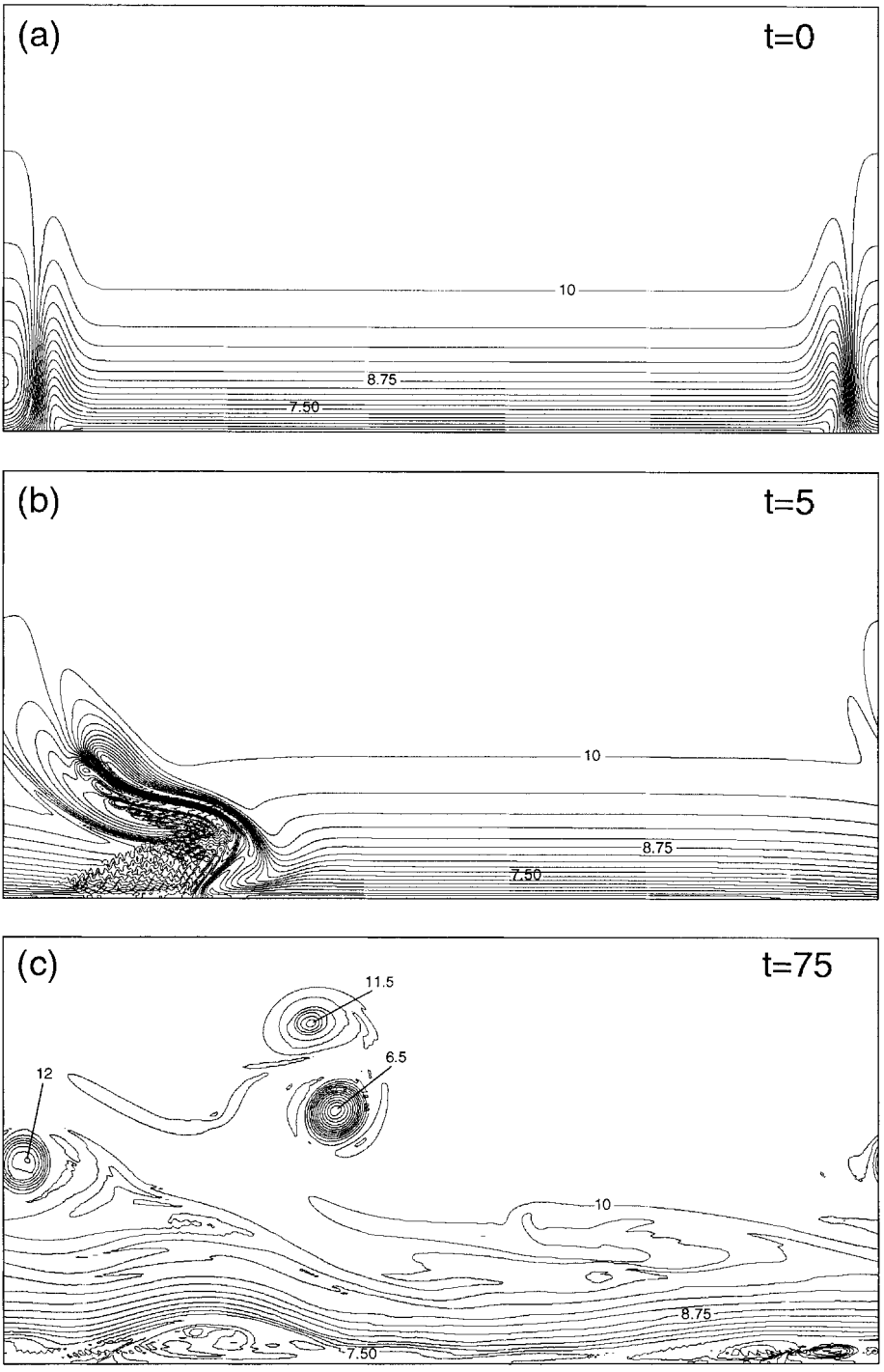

Figure 6. Potential vorticity contours for the second 1½ layer experiment of Section 4a ($W = 1$, contour interval of 0.25): (a–c) $t = 0$, $t = 5$, $t = 75$. Layer thickness contours for the second 1½ layer experiment of Section 4a ($W = 1$, contour interval of 0.1): (d) $t = 75$.

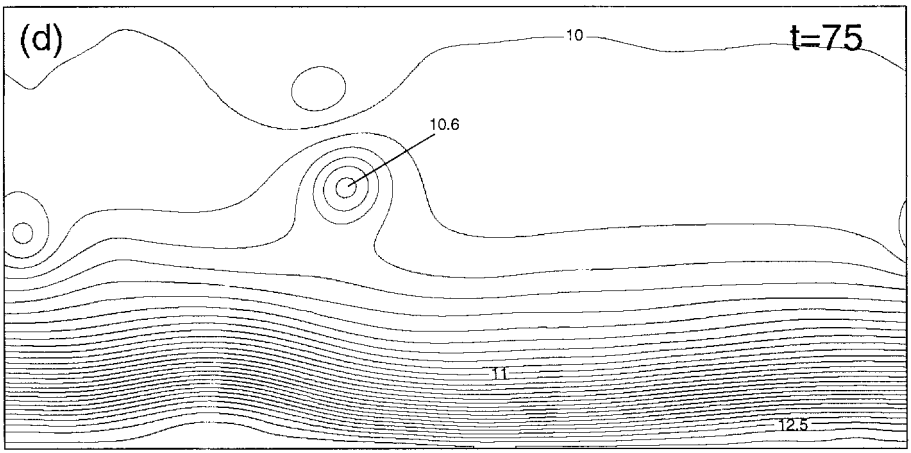

Figure 6. (Continued)

4. Separation of eddies from a wall current

In the numerical experiments of Section 2, we showed that entrainment occurs in an unstable boundary current when a small amplitude *periodic* perturbation is applied. In order to isolate the competing (or supplementary) detrainment process, a *localized* large amplitude disturbance (i.e., downstream variation) is assumed (below) as an initial condition in an otherwise *stable* boundary current.

a. Detrainment in a 1½ layer fluid

The initial PV distribution in Figure 4a is similar to the one in Figure 3a, except that PV is now continuous, and for computational reasons PV has a finite (but large) periodic downstream wavelength λ. The essential feature, however, is that the downstream width W of the region with strong downstream gradient in PV (and u) is small compared to λ. This initial PV was obtained (geostrophically) from the thickness field $h(x, y, 0)$, whose nondimensional value is

$$h(x, y, 0) = H + \Delta h e^{-y+1} [1 + y(1 + \tanh (x - \lambda/4))/2], \qquad 0 \le x \le \lambda/2 \tag{7}$$

$$h(x, y, 0) = H + \Delta h e^{-y+1} [1 + y(1 - \tanh (x - 3\lambda/4))/2], \qquad \lambda/2 \le x \le \lambda \tag{8}$$

$$h(x, y, t) = \text{periodic in } x, \tag{9}$$

where $\Delta h = 1$, $\lambda = 20$, $H = 10$, and with R_d again providing the length scale. If λ is large, the bracketed term in Eq. (7) has its smallest value in the "upstream" region at $x = 0$, and therefore this region has a maximum velocity closer to the wall than occurs downstream at $x = \lambda/2$.

The computational domain is configured as in the previous 1½ layer instability calculation (Section 2a), except that it is now twice as long ($\lambda = 20$); the channel width,

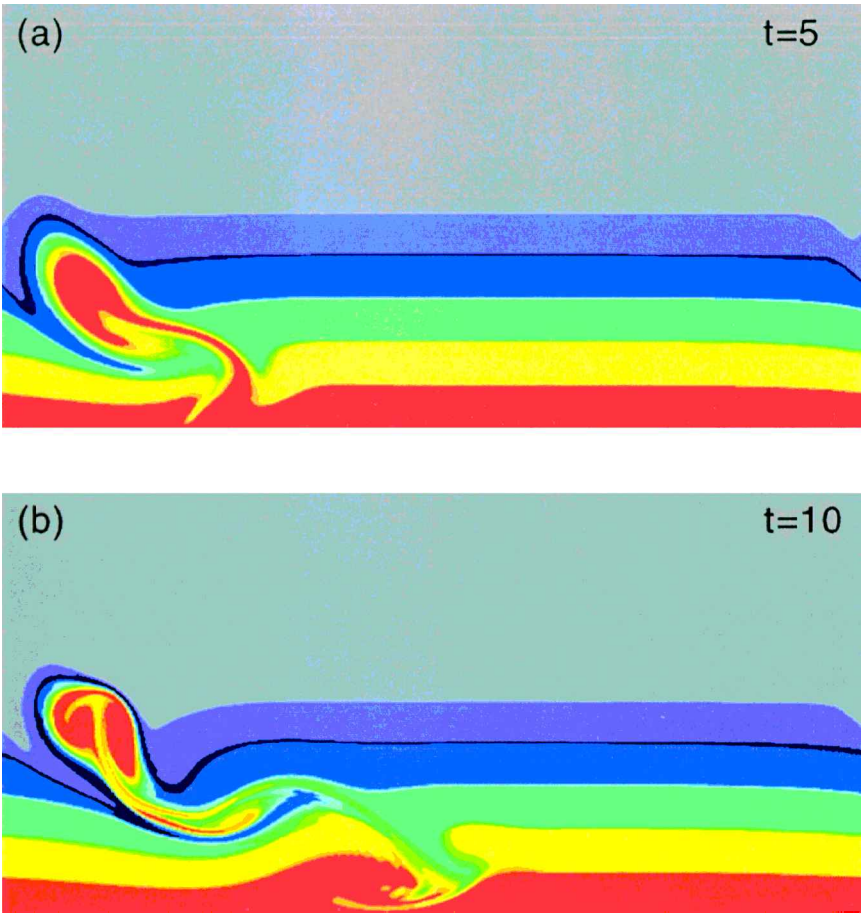

Figure 7. Same as Figure 5 for the second 1½ layer experiment of Section 4a ($W = 1$): (a–d) $t = 5$, $t = 10$, $t = 25$, $t = 50$.

grid spacing, and viscosity are unchanged, and the Rossby number is equal to 0.1. Although the value of h on the wall ($y = 0$) is initially constant at all x, the shallow water (MICOM) code allows $\partial h(x, 0, t)/\partial x \neq 0$ as the nonequilibrium state of Figure 4a evolves. The fast velocity u at $x = 0$, $y = 0$, converging on the slower u at $x = \lambda/2$, $y = 0$ leads to the expected [from the quasi-geostrophic theory (Fig. 3a, b)] potential vorticity "front" (at $t = 5$ in Fig. 4b). At $y = 0^+$, the large downstream convergence ($-\partial u/\partial x$) produces large $\partial v/\partial y$, large v, and large strain. As in the contour dynamical calculation, a plume of low potential vorticity is ejected from the wall region into the ambient high potential vorticity region. The plume tilts backwards relative to the rapidly propagating PV front near the wall, and at $t = 50$ (Fig. 4c) two strong low PV eddies are formed; the one farthest from the wall has a minimum PV = 8.5, and the one below it at $x \sim \lambda$ has a minimum PV = 7. These values indicate that the particles at these minima originate very close to the wall (min

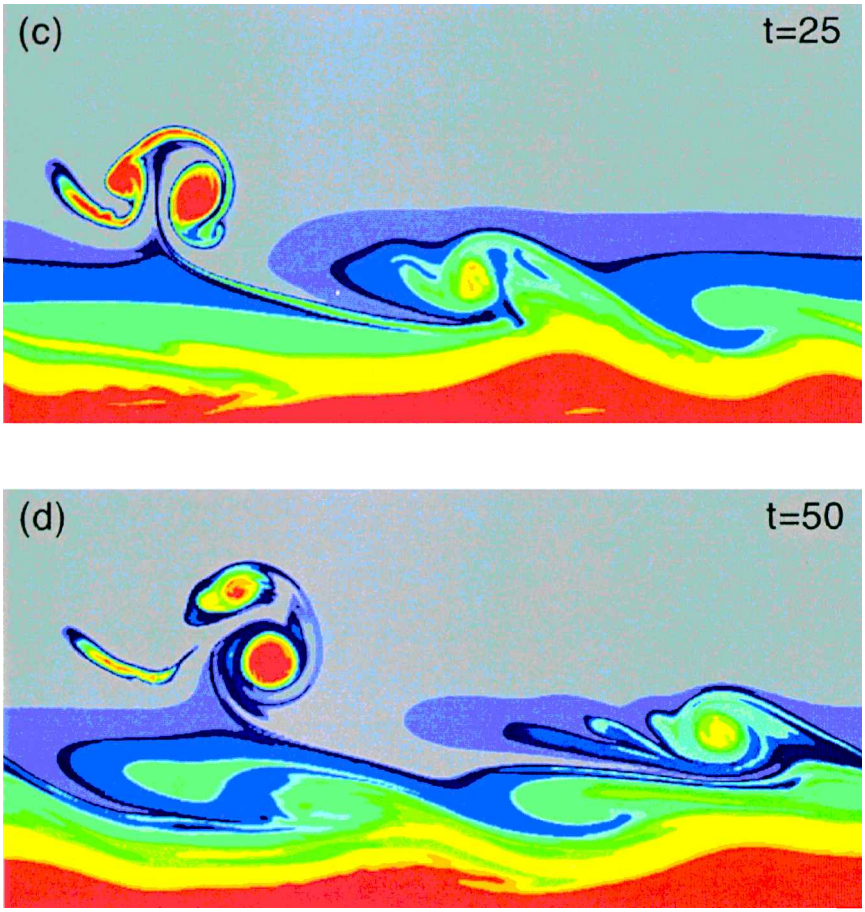

Figure 7. (Continued)

PV = 7 at $y = 0$ in Fig. 4a). The eddy of relatively small area with high PV = 11 also originates near $y = 0$, and forms as the fast upstream wall current of high potential vorticity is swept around the low PV plume. Fig. 4d ($t = 75$) indicates that the eddy farthest from the wall has hardly moved from its position at $t = 50$, and is clearly disconnected from the mean flow. Thus we conclude that even a 1½ layer coastal current, subjected to isolated perturbations with large downstream gradients, can evolve so that particles near the coast are ejected to large offshore distances, where they form separated eddies. This detrainment effect contrasts with the entrainment of exterior fluid produced by spatially periodic disturbances in an unstable boundary current. Under certain conditions, both effects can occur in different space-time regimes (see Section 4b for an example).

The separation of eddies can be better exhibited (Fig. 5) by means of a passive tracer injected at $t = 0$ over half the channel width, and such that there is a uniform (in x) band of color for every $\Delta y = 1$. The subsequent advection of the tracer was performed with the

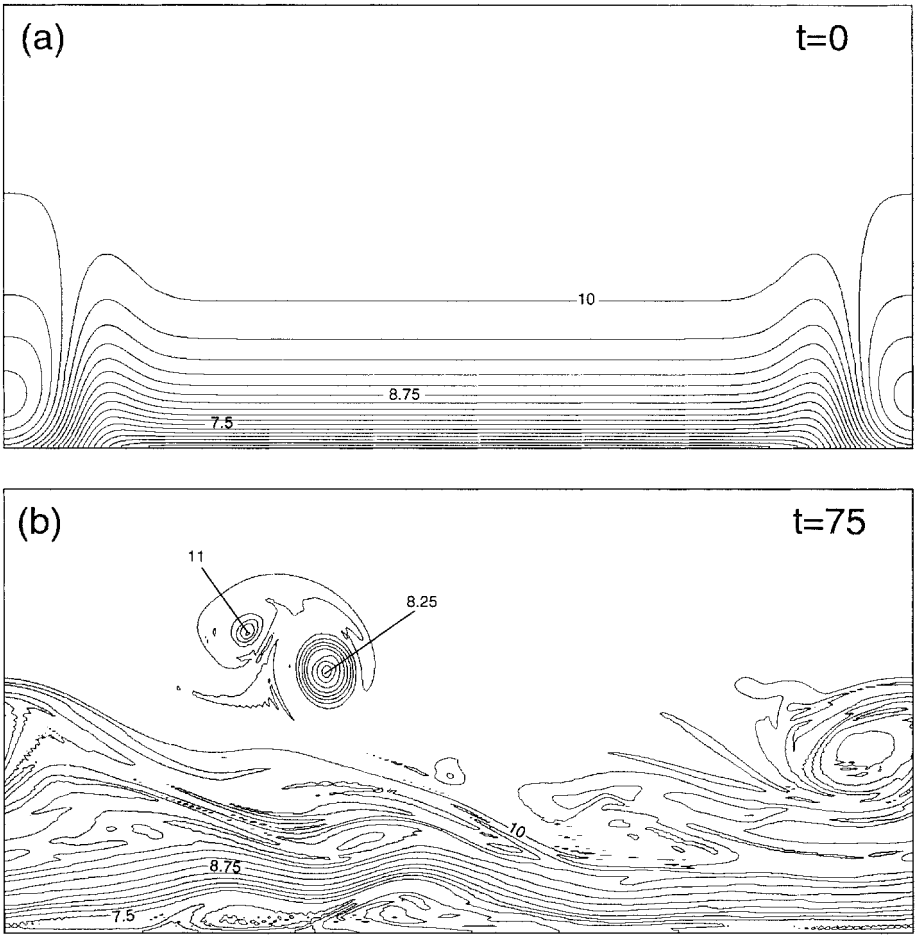

Figure 8. Potential vorticity contours for the third 1½ layer experiment of Section 4a ($W = 2$, contour interval of 0.25): (a–b) $t = 0$, $t = 75$.

MPDATA algorithm (Smolarkiewicz, 1984), which combines the smoothness properties of the upstream differencing scheme with the accuracy of space-centered schemes. At $t = 10$, we see the red layer near the wall being ejected by the plume; at $t = 25$, the latter starts to break up into eddies and, at $t = 50$, the separation is virtually complete.

The separation is even more dramatic for an initial PV state with a narrower relative width (W) of the front. The one shown in Figure 6a also has a smaller downstream width of the high PV domain; otherwise everything is the same as in the previous run. A numerically convenient initial condition for this is

$$h = H + \Delta h e^{-y}\left[1 + y\left(\tanh\left(\frac{x}{W}\right)^2 + \tanh\left(\frac{x-\lambda}{W}\right)^2 - 1\right)\right], \tag{10}$$

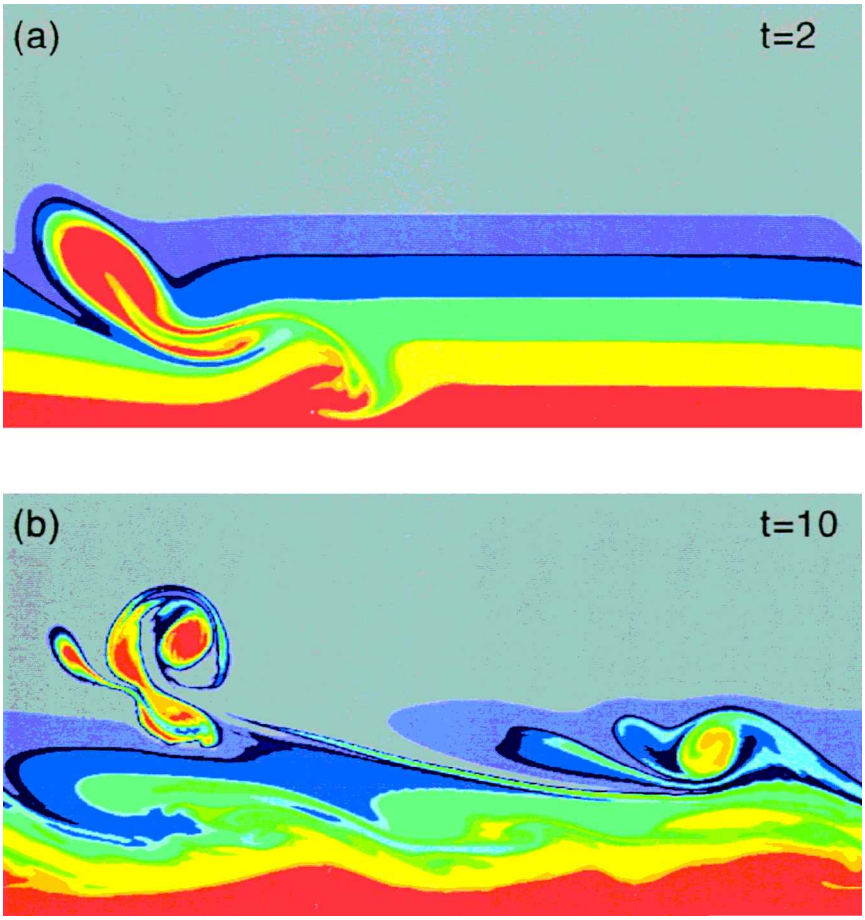

Figure 9. Same as Figure 5 for the fourth 1½ layer experiment of Section 4a ($\Delta h = 4$): (a–b) $t = 2$, $t = 10$.

and the associated initial (u, v) were computed (geostrophically) for $R_d = 1$, $\Delta h = 1$, $W = 1$, $H = 10$, $\lambda = 20$.

At $t = 5$ (Fig. 6b), the ejected plume contains dipolar potential vorticity anomalies that propagate to the far field by $t = 75$ (Fig. 6c), and a high PV anomaly appears at the edge of the wall current; the thickness field in Figure 6d shows that this is an anticyclone. The near-wall origin of the separated eddies is clearly shown by the passive tracer diagrams at $t = 5$, 10, 25, 50 (Fig. 7). When the front width is doubled ($W = 2$), other things being equal, the initial distribution of PV (Fig. 8a) evolves into a qualitatively similar state of detached eddies at $t = 75$ (Fig. 8b).

For $W = 5$ (not shown), potential vorticity frontogenesis similar to Figure 4b was observed at $t = 10$, but at $t = 75$, the maximum PV in the eddy farthest from the wall indicated that the corresponding parcel originated farther away from the wall than when

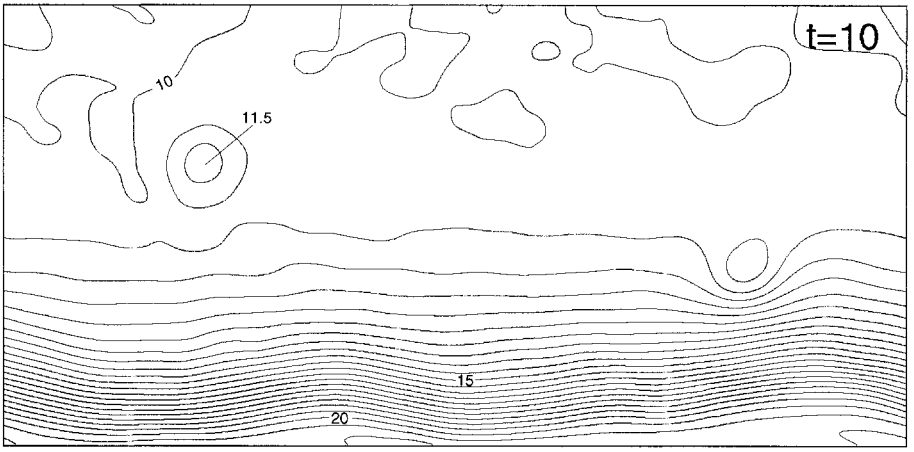

Figure 10. Layer thickness contours for the fourth 1½ layer experiment of Section 4a at $t = 10$ ($\Delta h = 4$, contour interval of 0.5).

$W = 2$. Eddy separation from the average wall jet was *not* observed in a run (not shown) with a strictly sinusoidal downstream initial variation (with large amplitude), although a front with a PV plume did form.

A strongly ageostrophic calculation was also made using the same h profile as in Figure 4a (with the initial u, v computed geostrophically), except that the value of $\Delta h = 4$ was much larger. The tracer diagrams at $t = 2$, 10 (Fig. 9) show that in this case the wall fluid is ejected into the far field much more rapidly, and Figure 10 shows that the thickness field at $t = 10$ contains a completely detached anticyclone.

b. Detrainment in an outcropping front

As in the nonoutcropping case of Section 4a, the assumed finite initial perturbation in the outcropping frontal model of Section 3b (Fig. 3c) might correspond to (inevitable) downstream variations in the structure of a boundary current connected to a source. Note that the requirement of constant (in x) total transport of the previous quasi-geostrophic 1½ layer model (Section 4a) is now removed, and the following calculations using multilayer density models should indicate whether the separation obtained in Section 4a with the nonoutcropping 1½ layer model occurs more generally.

The basic state [Eqs. (11)–(12)] is the same as for the instability case of Section 2b [Eqs. (5)–(6)], except that the latter are now modulated by a nonsinusoidal factor $A(x)$:

$$h_1 = \frac{A(x)}{3}(1 + \cos(\pi y/L_1)), \qquad y \le L_1 \tag{11}$$

$$h_2 = \frac{A(x)}{2}(1 + \cos(\pi y/(L_1 + L_2))), \qquad y \le L_1 + L_2. \tag{12}$$

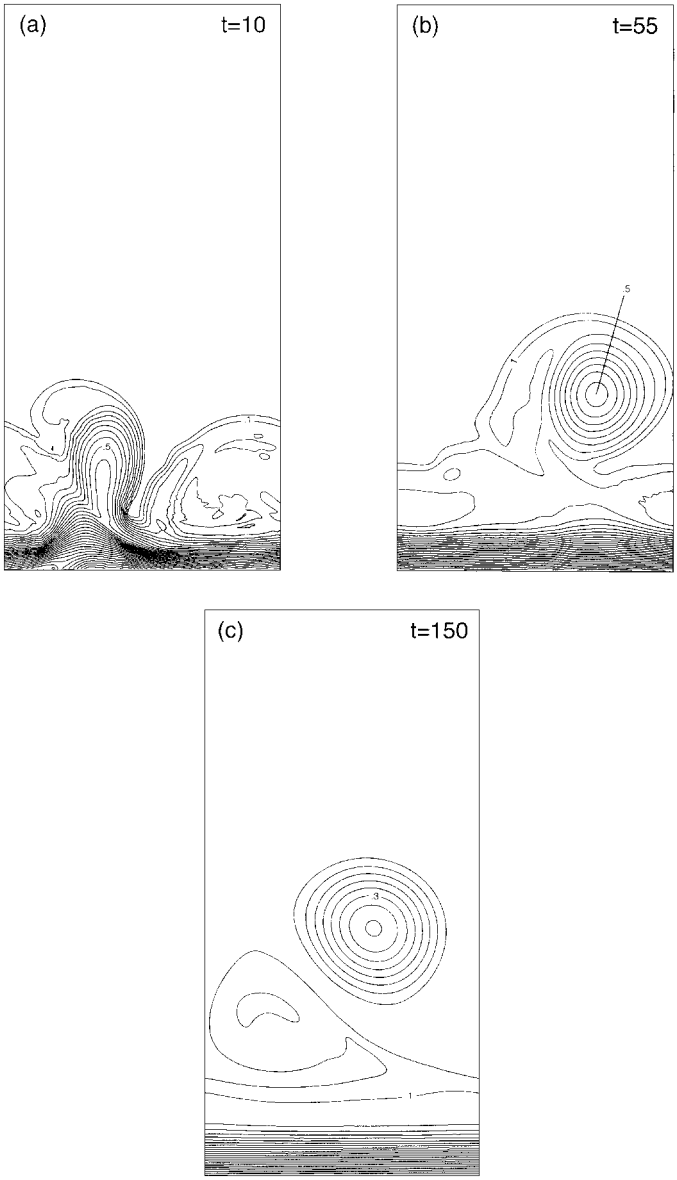

Figure 11. Layer thickness h_2 contours for the 3-layer outcropping front experiment of Section 4b (contour interval of 0.5): (a–c) $t = 10$, $t = 55$, $t = 150$.

A numerically convenient form is $A(x) = \tanh(x/W)^2 + \tanh((x - \lambda)/W)^2$, which is similar to the one used in Section 4a for the 1½ layer case (in Eq. 10), and $A(x)$ satisfies the computational periodicity condition $A(0) = A(\lambda)$. The associated *initial* (u, v) were computed (geostrophically) for $L_1 = 1, L_1 + L_2 = 2, R_d = 1, W = 1, H = 5, \lambda = 10$, and the

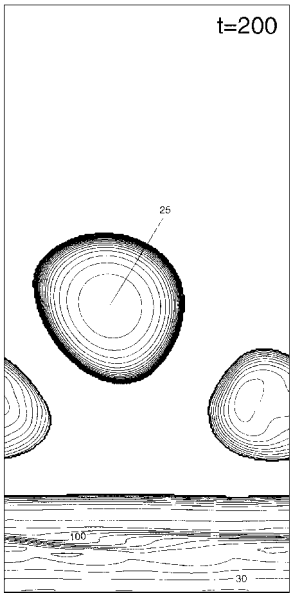

Figure 12. Potential vorticity contour for the outcropping front experiment of Section 4b at $t = 200$ (contour interval of 10).

computational width of the channel was doubled in order to keep the opposite boundary far away from the separated eddies.

As in the contour dynamical calculation, and in the 1½-layer experiments of Section 4a, the h_2-thickness contours display a steepening wave ($t = 10$, Fig. 11a) and the ejection of a plume of low potential vorticity from the wall region. The h_1-thickness contours, on the other hand, only exhibit small wave-like instabilities early on in the calculation and then return to a laminar state. Ejection of a first eddy in the middle density layer (h_2) occurs at $t = 55$ (Fig. 11b), and a second one (of weaker amplitude) is formed at $t = 150$ (Fig. 11c). The boundary current becomes laminar after the two eddies are completely separated (as illustrated by the mid-level potential vorticity contours of Fig. 12) and drift slowly upstream; upstream propagation was also observed in the laboratory experiments of Baey *et al.* (1995). By the end of the simulation ($t = 200$, Fig. 12), 27.3% of the original mass of the wall jet (layer 1 and 2 combined) is ejected into the two eddies.

In order to isolate the importance of various baroclinic effects in this experiment, several additional calculations were performed with almost identical initial conditions. In the first case, the upper layer is removed ($h_1 = 0$ everywhere) and, in this 2-layer model, the (single) front becomes unstable very rapidly, forming an anticyclone which is ejected from the main current as early as $t = 10$ (Fig. 13a); the small adjacent cyclonic circulation consists of a thin ring of upper layer fluid wrapped around lower layer fluid. By $t = 15$, a large volume of exterior fluid has been enclosed between the $h_2 = 0$ front and the boundary (Fig. 13b). This entrainment of outside fluid is completed when the dipolar eddy rotates and

moves toward the boundary ($t = 20, 25$; Fig. 13c, d) [in a process similar to that described in Section 2a and in Stern *et al.* (1997)]. In contrast to the 1½ layer experiments of the previous section, baroclinicity in the outcropping jet now plays a significant role in the entrainment/detrainment process. Detrainment, however, also occurs at a later time in this experiment when the returning dipole ($t = 25$, Fig. 13d) induces a blocking effect by $t = 30$ (Fig. 13e) and a new dipole is ejected at $t = 45$ (Fig. 13f). This time, as in Jungclaus (1999), the cyclonic partner dissipates, leaving only the anticyclone ($t = 70$, Fig. 13g). The further outward displacement of the anticyclone results from the presence in the lower layer of a small dipole (Fig. 14) below the upper layer eddy.

For this particular outcropping front, in contrast to the 1½ layer experiments of Section 4a, a finite lower layer depth is necessary for the entrainment/detrainment process to occur. This was demonstrated by the second and third additional sensitivity experiments, in which the lower layer depth (of the 2- and 3-layer experiments, respectively) was made infinitely deep ($H = \infty$). In both these cases (not shown), there is insignificant outward excursion of the boundary current, no eddy formation, and the current becomes laminar after a short time.

5. Conclusions

Finite amplitude numerical calculations for a laminar wall jet initialized with sinusoidal downstream disturbances show that barotropic and/or baroclinic instability effects can produce entrainment of offshore fluid, but these effects are insufficient to completely separate an eddy from the jet. In order to produce the latter, a supplementary dynamical process is needed. Laboratory and numerical experiments strongly suggest that the blocking induced by the generic downstream variation in a wall jet emerging from a source, or with the aperiodic downstream variation of wave disturbances, could be responsible for eddy separation. In the ocean, other factors such as local topographic variations may also create a blocking wave which induces separation. The formation of blocking waves on a boundary current, first investigated using contour dynamical calculations (Stern, 1980; 1986), suggest that this process will eventually lead to a separated eddy. We, therefore, investigated numerically the long time evolution of the blocking created by a large amplitude local disturbance of unspecified origin in the wall jet. The numerical calculations are qualitatively consistent with the blocking effect predicted by the longwave theory of Stern (1980, 1986). In some cases, the blocking can be strong enough to cause boundary fluid to be detrained by means of an eddy which completely pinches off from the remaining coastal current. It was shown that eddy separation (or detrainment) can occur with one or more active layers. Entrainment can also occur in regions where periodic barotropic/baroclinic instabilities exist. More realistic models need to be considered to determine the parametric conditions under which each of these effects occur, and their coupling. Of particular interest would be numerical experiments with a source strength that can be decreased and increased in a controlled manner to realize the downstream convergences assumed herein.

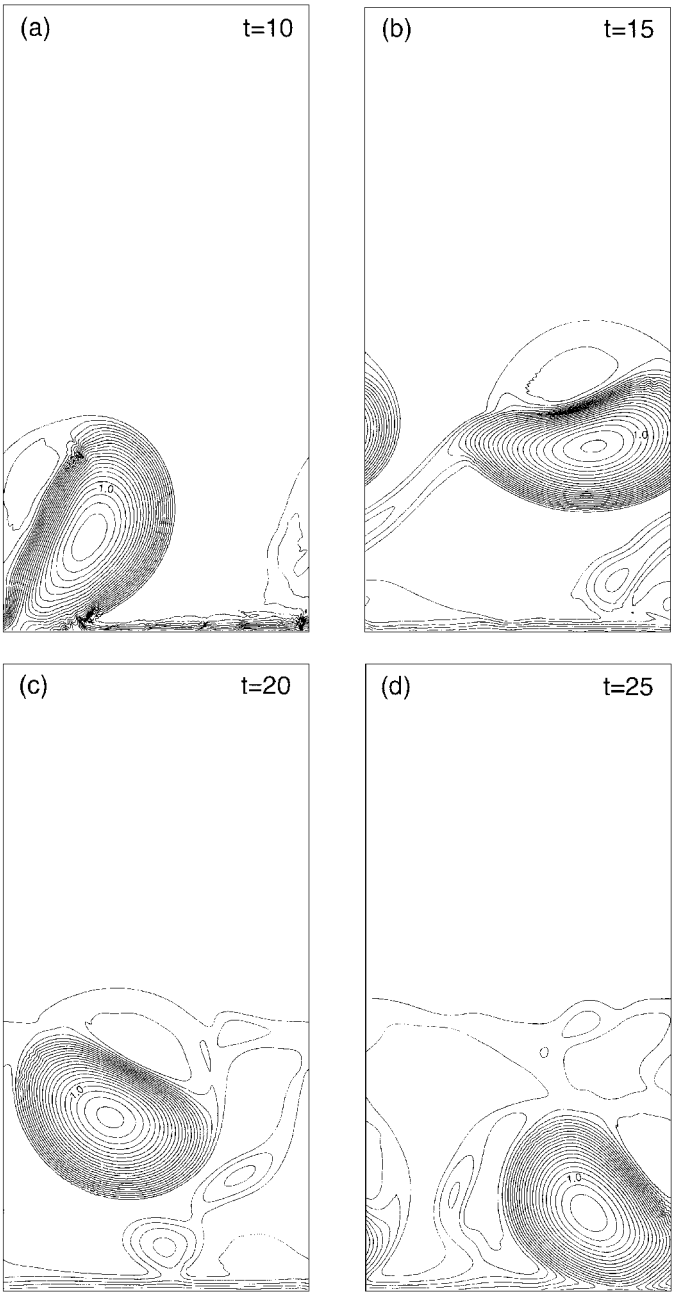

Figure 13. Layer thickness contours for the 2-layer outcropping front experiment of Section 4b (contour interval of 0.5): (a–g) $t = 10$, $t = 15$, $t = 20$, $t = 25$, $t = 30$, $t = 45$, $t = 70$.

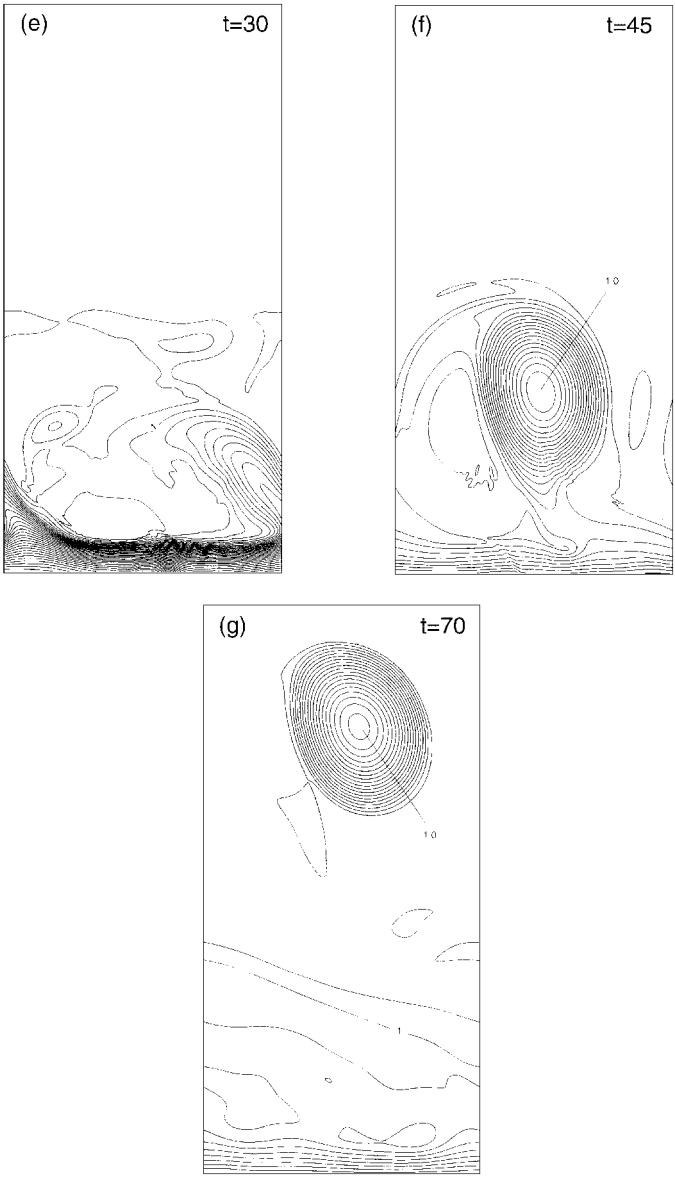

Figure 13. (Continued)

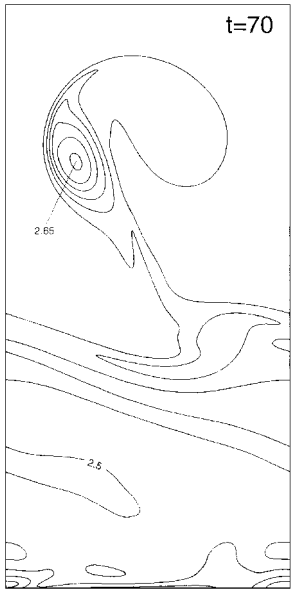

Figure 14. Lower layer potential vorticity at $t = 70$ for the 2-layer outcropping front experiment of Section 4b (contour interval of 0.05).

Acknowledgments. Most of this work was performed at the 1998 Program of Summer Study in Geophysical Fluid Dynamics held at the Woods Hole Oceanographic Institution. Melvin E. Stern was supported by the National Science Foundation through Grant OCE-9529261 and Eric P. Chassignet by the National Science Foundation through Grant OCE-9711186.

REFERENCES

Baey J-M., D. Renouard and G. Chabert d'Hieres. 1995. Preliminary results about the stability of an intermediate water current. Deep Sea-Res., *42,* 2063–2073.

Bleck, R. and D. B. Boudra. 1986. Wind-driven spin up in eddy-resolving ocean models formulated in isopycnic and isobaric coordinates. J. Geophys. Res., *91,* 7611–7621.

Bleck, R. and E. P. Chassignet. 1994. Simulating the oceanic circulation with isopycnic coordinate models, *in* The Oceans: Physical and Chemical Dynamics and Human Impact. The Pennsylvania Academy of Science, 17–39.

Bower, A. B., L. Armi and J. Ambar. 1997. Lagrangian observations of Meddy formation during a Mediterranean undercurrent seeding experiment. J. Phys. Oceanogr., *27,* 2545–2575.

Flierl, G. R., P. Malanotte-Rizzoli and N. J. Zabusky. 1987. Nonlinear wave and coherent vortex structures in barotropic β-plane jets. J. Phys. Oceanogr., *17,* 1408–1438.

Griffiths, R. W. and P. F. Linden. 1981. The stability of buoyancy-driven coastal currents. Dyn. Atmos. and Oceans, *5,* 281–306.

Haidvogel, D. B., A. Beckman, and K. S. Hedstrom. 1991. Dynamical simulations of filament formation and evolution in the coastal transition zone. J. Geophys. Res., *96,* 15017–15040.

Jiang, L. and R. W. Garwood. 1998. Effects of topographic steering and ambient stratification on overflows on continential slopes. J. Geophys. Res., *103,* 5459–5476.

Jungclaus, J. H. 1999. A three-dimensional simulation of the formation of anticyclonic lenses (Meddies) by the instability of an intermediate depth boundary current. J. Phys. Oceanogr., *29,* 1579–1598.

Pratt, L. J., K. R. Helfrich and E. P. Chassignet. 2000. Hydraulic adjustment to an obstacle in a rotating channel. J. Fluid Mech., *404,* 117–149.

Smolarkiewicz, P. 1984. A fully multidimensional positive definite advection transport algorithm with small implicit diffusion. J. Comput. Phys., *54,* 325–362.

Stern, M. E. 1980. Geostrophic fronts, bores, breaking and blocking waves. J. Fluid Mech., *99,* 687–703.

—— 1986. On the amplification of convergences in coastal currents and the formation of squirts. J. Mar. Res., *44,* 403–421.

—— 1999. Separation of a mid-level density current from the bottom of a continental slope. Proc. National Acad. Sci., *96,* 1206–1211.

Stern, M. E., E. P. Chassignet and J. A. Whitehead. 1997. The wall jet in a rotating fluid. J. Fluid Mech., *335,* 1–28.

Wygnanski, I., Y. Katz and E. Horev. 1992. On the validity of various scaling laws to the turbulent wall jet. J. Fluid Mech., *234,* 669–690.

Received: *10 November, 1998;* revised: *3 January, 2000.*